Wholefield Optical Metrology:

Surface Displacement Measurement

C.R. Coggrave

Phase Vision Ltd
http://www.phasevision.com/

1 Introduction

Conventional methods of measuring physical parameters such as surface strain, displacement, and profile utilise strain gauges, dial gauges and other mechanical or electrical sensing devices. Although these point-wise methods can potentially produce high-precision measurements their drawbacks include the requirement for contact with the surface under test and the localised measurement area. In general, large numbers of separate measurements are required to build up an overall picture of the physical parameter, however, when the required number of sensors exceeds 10^2-10^3 the cost typically becomes prohibitive. There has thus been much interest in developing *whole-field* (or full-field) non-contact metrology techniques that are able to provide measurements over large areas of the object surface at any one time to overcome the laborious procedure of point-wise measurement. Optical metrology methods such as speckle interferometry and optical profilometry provide an attractive solution for many applications and can provide whole-field information equivalent to more than 10^5 independent point-wise sensors. Sophisticated digital cameras with high spatial resolution (i.e. number of pixels), high temporal resolution (i.e. frame rate), and high accuracy (i.e. number of bits) have in many applications replaced photographic plates, thus enabling optical techniques to be adopted more easily.

Whole-field optical metrology is a broad subject area encompassing the measurement of physical properties of smooth or rough objects that can be opaque or transparent. The scope of this paper is limited, however, to engineering interest in surface displacement of *opaque* objects. Applications are introduced that provide a wide choice of sensitivities and dynamic range. The high sensitivity offered by interferometric techniques is well suited to displacement measurement where limited dynamic range is required. In particular, speckle interferometry offers strong potential for integrated systems that can be used outside of the laboratory due to relatively low cost components, variable sensitivity, and relative ease with which it can be set-up and used.

This paper presents the most popular whole-field optical methods for measuring the displacement and displacement-gradient of test surfaces. The Cartesian components of the displacement vector $\mathbf{d}(P)$ at point $P(x, y)$ on the test surface are denoted by $u(x, y)$, $v(x, y)$ and $w(x, y)$, respectively.

2 Smooth wavefront interferometry

Coherent signal processing requires that information about both the amplitude and phase of wavefronts be measured. However, all practical light detectors respond only to light intensity and it is therefore necessary to convert the phase information to variations in intensity for measurement purposes. *Interferometry* is a standard technique used to accomplish this task. A second coherent wavefront of known amplitude and phase (the *reference* wave) is added to the unknown wavefront (the *object* wave); the intensity of the sum then depends on both the amplitude and phase of the original wavefront.

Smooth wavefront interferometry refers to those interferometry techniques based only on the "smooth" wavefronts produced when all the optical elements in a system, including the surface under test, have a negligible surface roughness when compared to the wavelength of light. By contrast, optical techniques involving rough surfaces compared to the wavelength of light (e.g. holography and speckle interferometry) produce "speckle" wavefronts and are discussed later.

We begin our analysis by describing the spatio-temporal distribution of a linearly polarized plane harmonic wave with angular frequency $\omega = 2\pi\nu$ and initial phase φ at the origin. If the wavefront is propagating in the direction of the wavevector $\mathbf{k}$ then the complex amplitude is given by

$$A(\mathbf{r},t) = a_0 e^{i(\mathbf{k}\cdot\mathbf{r}-\omega t+\varphi)} \tag{1}$$

Removing the spatial dependence for clarity, the intensity, or *irradiance*, of a general wave is given by

$$I(t) = c\varepsilon\left\langle A(t)A^*(t)\right\rangle \tag{2}$$

where c is the speed of the wave propogation, ε is the electric permittivity of the transmission medium, $\langle\rangle$ is the time average operator, and * denotes the complex conjugate. Since we will only be concerned with relative intensities within the same medium it is useful to neglect the scaling constants and set

$$I(t) = \left\langle A(t)A^*(t)\right\rangle \tag{3}$$

A practical light sensor, however, cannot follow the frequency of light and therefore is unable to measure the instantaneous intensity. The sensor thus integrates over a finite measurement time T_m

$$I = \lim_{T_m \to \infty} \frac{1}{T_m} \int_{-T_m/2}^{T_m/2} A(t')A^*(t')dt' \tag{4}$$

Typically the integration period T_m extends over many periods of oscillation (i.e. $T_m \rangle\rangle 2\pi/\omega$) hence the measured intensity is simply

$$I = |A|^2 \tag{5}$$

Consider then an object wave $A_1 = a_1 e^{i\phi_1}$ and reference wave $A_2 = a_2 e^{i\phi_2}$, the intensity of the sum is given by

$$\begin{aligned} I &= (A_1 + A_2)(A_1^* + A_2^*) \\ &= a_1^{\,2} + a_2^{\,2} + 2a_1 a_2 \cos(\phi_1 - \phi_2) \end{aligned} \tag{6}$$

The first two terms, the *self-interferenc*e terms, depend only on the intensities of the two waves and represent noise terms that we have to suppress or discard as their presence in the final analysis leads to poor signal-to-noise ratios. The third term, however, depends on their relative phases and thus encodes the phase information of the unknown object wavefront.

A useful alternative notation is

$$I = I_0 + I_M \cos\Delta\phi \tag{7}$$

where $I_0 = I_1 + I_2$ and $I_M = 2\sqrt{I_1 I_2}$, where we define $I_1 = A_1 A_1^*$, $I_2 = A_2 A_2^*$, and $\Delta\phi = \phi_1 - \phi_2$.

A highly useful parameter in evaluating the performance of a system is the visibility or contrast of the interference pattern and is defined as

$$V = \frac{I_{\max} - I_{\min}}{I_{\max} + I_{\min}} \tag{8}$$

where $I_{\max} = I_0 + I_M$ and $I_{\min} = I_0 - I_M$. Hence, the intensity is often expressed in terms of visibility as

$$I = I_0(1 + V\cos\Delta\phi) \tag{9}$$

3 Holographic interferometry

Advances in holography have resulted in two powerful interferometric techniques being developed that are suitable for non-destructive testing applications, and particularly measurements of the deformation of diffusely reflecting opaque objects. In contrast to a photograph where the light reflecting off the surface carries with it information about the irradiance but nothing about the phase of the wavefront that once emanated from the object, a hologram records both the irradiance and phase information. Following development of the holographic plate, the image is reconstructed by diffracting a coherent beam using the transparent hologram.

In the *double exposure method* of holographic interferometry two wavefronts scattered by the same object are mixed with a reference wavefront and recorded consecutively onto the same holographic plate. The plate is first exposed to the object wavefront scattered by the undisturbed object mixed with the reference wavefront (figure 1), then after a change in physical parameter (e.g. object shape due to deformation) the plate is exposed once again to the modified object wavefront mixed with the reference wavefront (figure 2). Following development of the plate (figure 3), the reconstructed waves overlap and interfere to form a fringe pattern indicative of change in optical path length between the two object states. If the spatial variation of the interference phase over the observed reconstructed surface is low, the intensity distribution represents the irradiance of the object, modulated by a cosine fringe pattern as expressed in equation 9.

In *real-time holographic interferometry* the object under test is left in its original position throughout and only the object wavefront scattered by the undisturbed object mixed with the reference wavefront is recorded on the holographic plate. Following development of the plate it must be returned to its original position with sub-wavelength precision such that the reconstructed virtual image wavefront coincides exactly with the wavefront scattered directly by the object (figure 4). During testing of the object, superposition of the scattered wavefront with the reconstructed wavefront results in a live interference pattern (or *interferogram*) that is a function of the physical parameter under investigation. Video equipment is often used to make real-time recordings of the interferogram.

The displacement vector $\mathbf{d}(P)$ of point $P(x,y)$ on the object surface produces an optical path difference $\delta l(P)$ given by[6]

$$\delta l(P) = \mathbf{d}(P) \cdot \left[\mathbf{b}(P) - \mathbf{s}(P)\right] \tag{10}$$

where $\mathbf{s}(P)$ and $\mathbf{b}(P)$ are the unit vectors in the illumination direction and observation direction respectively. The interference phase is related to the path difference by

$$\Delta\phi(P) = \frac{2\pi}{\lambda}\delta l(P) \tag{11}$$

so that we get the general formula

$$\Delta\phi(P) = \mathbf{d}(P) \cdot \mathbf{e}(P) \tag{12}$$

where $\mathbf{e}(P)$ is the so called *sensitivity vector*

$$\mathbf{e}(P) = \frac{2\pi}{\lambda}\left[\mathbf{b}(P) - \mathbf{s}(P)\right] \tag{13}$$

In order to determine the components of a displacement vector from an evaluated interferogram we have to discriminate between a constant sensitivity vector and a sensitivity vector that varies over the interferogram. In the latter case it may be sufficient to estimate the maximum error introduced by the extreme sensitivity vectors of the actual holographic set-up. In most engineering problems the deformation can be predicted and it is therefore good practice to configure the holographic set-up with maximum sensitivity in the expected direction of deformation. Abramson developed the so-called *holo-diagram*[7] as an aid to designing holographic set-ups for optimum sensitivity.

Several excellent books[8-10] are available providing further information on these holographic techniques, and many others.

4 Speckle interferometry

The granular appearance known as the *speckle effect* observed when coherent light is reflected from a diffuse surface can be a real practical nuisance in coherently illuminated systems. In holographic interferometry, for example, the speckle pattern is regarded as background noise. The development of speckle metrology[11-13] is historically linked to the realization that the grainy appearance of the reconstructed holographic images could be used to convey additional information.

The simplest speckle metrology technique is *speckle photography*[14] in which a single coherent beam is used to illuminate the object. Speckle patterns obtained before and after deformation are compared using the speckle grains recorded on the photographic plate as markers to monitor changes in the physical parameter. The principle sensitivity of speckle photography is in the direction normal to the optical axis (i.e. in-plane displacement). The displacements generally have to be larger than the speckle size, which can be controlled by the detector aperture. This is not strictly an interference method, however, the evaluation stage usually involves interference patterns.

Speckle interferometry[8,15,16] involves the interference of two optical waves in which at least one is a speckle field. It provides a powerful technique for the measurement of deformations or contours of rough surfaces depending on the geometry of the illumination. Speckle interferometry is closely related to holographic interferometry and is equally sensitive. Whilst speckle interferometry does not require the recording of a hologram, the fringe patterns obtained normally have a lower signal to noise ratio than those produced in holographic interferometry. Generally speaking, speckle interferometers can be divided into two categories, depending on whether two speckle fields (e.g. in-plane and shearing interferometry), or one speckle field and a smooth reference beam (e.g. out-of-plane interferometry), are mixed to form the interference pattern.

The most important technique of speckle interferometry is *digital speckle pattern interferometry* (DSPI), originally called *electronic speckle pattern interferometry* (ESPI), and also known by the names *electronic holography* and *digital holography*. Electronic speckle pattern interferometry[17] emerged in the 1970s as a method aimed

at combining optics and electronics by using standard TV or CCD cameras rather than holographic or photographic plates to eliminate the slow and cumbersome chemical processing of photographic emulsions. Co-linear reference and object wavefronts are required together with an imaging system in order to produce interference patterns suitable for the relatively low-resolution cameras.

Speckle interferograms obtained by superposition of a reference beam do not contain fringes as in classical interferometry since the phase of each speckle is statistically independent. However, each speckle within the image plane of the detector can be considered as an independent interferogram that can be expressed using classical interferometry as in equation 7. The phase distribution in a speckle interferogram can therefore be described by a uniform randomly distributed variable over the range $[0, 2\pi]$.

The measured physical parameter can be visualised by so-called *correlation fringes* obtained, for instance, by calculating the square of the difference in the intensity distributions (primary interferograms) recorded before and after deformation of the object. From equation 7 the intensity of each speckle grain (formed by the superposition of the object and reference beams) in the primary interferogram recorded with the object in its reference state is given by

$$I_i = I_0 + I_M \cos\phi \tag{14}$$

where ϕ is the random initial phase. Assuming that deformation of the object changes the phase but not the amplitude, the intensity of each speckle grain recorded in the deformed state is given by

$$I_d = I_0 + I_M \cos(\phi + \Delta\phi) \tag{15}$$

where $\Delta\phi$ is the phase change due to deformation. The square of the difference is therefore

$$\begin{aligned}(I_i - I_d)^2 &= \left[2I_M \sin\left(\phi + \frac{\Delta\phi}{2}\right) \sin\frac{\Delta\phi}{2} \right]^2 \\ &= 2I_M^2 \sin^2\left(\phi + \frac{\Delta\phi}{2}\right)\left(1 - \cos\Delta\phi\right)\end{aligned} \tag{16}$$

The low frequency $\cos\Delta\phi$ term modulates the high frequency speckle noise to produce grainy correlation fringes. Typically these fringes represent contours of constant displacement component, or depth, depending on the optical arrangement

used to acquire the speckle patterns. Dedicated systems have been commercially available for several years that use electronic subtraction and rectification to calculate and display the correlation fringes in real-time; such systems are well suited for qualitative analysis of object behaviour. Although intensity based techniques such as correlation fringes are sometimes also used for quantitative analysis, methods based on phase-shifting techniques are generally more appropriate.

There are many optical configurations used in speckle interferometry. Most of them are two-beam systems with each wavefront coming from a single light source and their paths separated by amplitude division. The most common arrangements for measuring surface displacement and displacement-gradient measurement are described in sections 5 to 7.

5 Out-of-plane speckle interferometry

Measurement of the out-of-plane displacement component *w* with speckle interferometers can be performed using either a speckle-wavefront or smooth-wavefront reference beam. The latter method has so far been the most popular and a common interferometer arrangement is shown in figure 5. The test surface is illuminated by the object beam parallel to the *x*-*z* plane and imaged onto the detector surface through a lens arrangement. The smooth-wavefront reference beam is brought onto the optical-axis using the beam combiner and superimposed with the speckle image of the object at the detector.

There have been many variations on this scheme to reduce the secondary reflections of the reference wave. For example, wedge[18] and cube beamsplitters have been used to introduce the reference beam, as well as monomodal optical fibre. In addition many arrangements introduce the reference beam before the imaging lens.

From equation 13, the sensitivity vector $\mathbf{e}(P)$ at point P in plane *x*-*z* on the test surface is given by equation 17, where θ is the object beam angle of incidence to the surface normal.

$$\mathbf{e}(P) = \frac{2\pi}{\lambda}\begin{bmatrix} \sin\theta \\ 0 \\ 1+\cos\theta \end{bmatrix} \tag{17}$$

In the plane *x*-*z*, the interferometer has zero sensitivity to the in-plane displacement component *v*, with negligible sensitivity above and below this plane for small regions of interest. For general operation, it is desirable to minimise the sensitivity to in-plane displacement component u by keeping θ as small as possible. Hence, for an illumination beam at normal incidence, adjacent coherence fringes correspond to an out-of-plane displacement of $\lambda/2$. The distance between the test surface and the effective source of the object beam should be maximised so that variations in θ, and thus variations in the sensitivity vector, are minimised across the region of interest. It should be noted that plane wavefronts would be required to achieve completely uniform sensitivity vectors, however, for many practical applications this approximation is acceptable. Wan Abdullah et al.[19] provide a detailed analysis of the errors introduced by this approximation.

High sensitivity to out-of-plane displacement can be a hindrance when measuring large deformations since high fringe densities prevent good quantitative spatial analysis of the interferogram. For example, the upper limit for a 512 × 512 pixel CCD detector is approximately 20 fringes thus limiting the maximum deformation that can be reliably measured to approximately 7 μm. Several methods for reducing the sensitivity have been reported, including for example, two-beam illumination with a small angle between the beams[20], oblique incidence and observation[21], and longer-wavelength lasers[22].

6 In-plane speckle interferometry

The double-illumination system[23] shown in figure 6 for measuring in-plane displacement components uses two coherent beams of light at angles θ_1 and θ_2 either side of the normal. The two beams generate their own speckle patterns that combine by superposition, and the scattered light is imaged on to the detector. It can be shown that the resultant sensitivity vector for such double-illumination arrangements is given by

$$\mathbf{e}(P) = \frac{2\pi}{\lambda}\left[\mathbf{s}_2(P) - \mathbf{s}_1(P)\right] \tag{18}$$

where $\mathbf{s}_1(P)$ and $\mathbf{s}_2(P)$ are the unit vectors along the illumination directions. The sensitivity vector at point P in plane *x*-*z* on the test surface is therefore given by

$$\mathbf{e}(P) = \frac{2\pi}{\lambda}\begin{bmatrix} \sin\theta_1 - \sin(-\theta_2) \\ 0 \\ \cos\theta_1 - \cos(-\theta_2) \end{bmatrix} \tag{19}$$

As with the optical arrangement discussed in section 5, there is negligible sensitivity to in-plane displacement component *v*. Out-of-plane sensitivity is zero at all points on the object surface where the illumination beams are symmetrical about the normal ($\theta = \theta_1 = \theta_2$) and the in-plane sensitivity component simplifies to

$$e_x = \frac{4\pi}{\lambda}\sin\theta \tag{20}$$

The presence of divergent illumination beams results in small variations in the sensitivity vector across the region of interest and is minimised by increasing the distance between the effective source position of the illumination beams and test surface. The presence of the $\sin\theta$ term in equation 20 enables the sensitivity to in-plane displacement u to be changed by varying the illumination direction.

Correlation fringes indicate contours of equal in-plane displacement parallel to the plane containing the two illumination beams. Hence, measurement of in-plane displacement component *v* along the *y*-axis would require that the illumination beams be arranged parallel to the *y*-*z* plane. In general, fringe quality is lower to that of a uniform reference system due to the speckle statistics. Since speckle decorrelation limits the displacement range that may be measured, large in-plane displacements

must be measured by integrating incremental speckle displacements for which the decorrelation remains small.

7 Speckle shearing interferometry

Electronic speckle-shearing pattern interferometry (ESSPI) was first suggested by Leendertz et al.[24] and has evolved into an essential tool for measuring the partial derivative of displacement of rough surfaces. A simple speckle shear arrangement is shown in figure 7 that uses a single illumination beam and a Michelson interferometer to perform shearing of the wavefront. A small tilt in the angle of one of the mirrors produces a constant linear shear δx resulting in two superimposed images of the object on the detector that combine coherently to generate a third speckle pattern. Each point in the image plane therefore receives a contribution from two points $P_1(x, y)$ and $P_2(x + \Delta x, y)$ on the test surface, where the object plane shear Δx is related to the image plane shear δx through the magnification of the imaging lens. One of these mutually shifted images can be regarded as the reference wavefront and the other the object wavefront, and hence this approach is known as *self-reference*.

As in the previous methods, the image captured after deformation is subtracted from the reference image captured before deformation. From equation 12, the phase change in the contributions from points P_1 and P_2 due to the deformation of the test surface are given by equations 21 and 22, respectively.

$$\delta\phi_1 = \mathbf{d}(P_1) \cdot \mathbf{e}(P_1) \tag{21}$$

$$\delta\phi_2 = \mathbf{d}(P_2) \cdot \mathbf{e}(P_2) \tag{22}$$

If we let the Cartesian components of the displacement vectors $\mathbf{d}(P_1)$ and $\mathbf{d}(P_2)$ be (u, v, w) and $(u + \Delta u, v + \Delta v, w + \Delta w)$, respectively, then the interference phase of the combined speckle patterns is $\Delta\phi = \delta\phi_1 - \delta\phi_2$ is given by

$$\Delta\phi = \frac{2\pi}{\lambda}\left[\Delta w(1 + \cos\theta) - \Delta u(\sin\theta)\right] \tag{23}$$

Dependence on the in-plane displacement component u is dropped if the illumination beam is arranged normal to the object surface, i.e. $\theta = 0$. Hence, provided that the object plane shear Δx is small compared to the surface displacement then the change in phase can be expressed in terms of the partial derivative of out-of-plane displacement with respect to the *x*-direction.

$$\Delta\phi \approx \frac{2\pi}{\lambda}\left[(1 + \cos\theta)\frac{\partial w}{\partial x}\right]\Delta x \tag{24}$$

The shear interferogram displays only abrupt changes in displacement as contributions due to rigid body movement of the test surface cancel. Alternative methods exist to create the sheared image and include: (a) the use of a glass wedge placed in front of one half of the imaging lens[25]; (b) the use of two tilted glass plates[26] placed in front of the imaging lens; (c) the use of a binary grating[27] placed in front of the imaging lens; (d) the use of a double wedge or Fresnel bi-prism[28] placed in front of the imaging lens; and (e) the use of multiple apertures in conjunction with a lens and defocusing[29,30]. Krishna Murphy et al. [31] describe some of the drawbacks of these techniques and introduces the split-lens shearing method as an alternative.

Due to the common beam path, the shearing interferometer provides a simple arrangement with good immunity to the effects of turbulence and vibration for small shear amounts, and therefore is well suited to industrial applications. The shearing speckle interferometer is commonly employed for detecting defects in surfaces, where the defect produces a steep out-of-plane displacement gradient identified by the close grouping of fringes. Increasing the shear distance improves gradient sensitivity, whilst at the same time reducing spatial resolution. Significant rigid body movement or turbulence may result in speckle decorrelation reducing fringe contrast to unacceptable levels.

8 Summary

This paper has presented a brief description of the most popular whole-field optical techniques for measuring surface displacement and surface profile. However, these represent only a small fraction of the wide range of optical arrangements that are described in the literature.

Digital speckle pattern interferometry has been widely adopted as the standard technique for displacement measurement in many application areas. Its acceptance has been fuelled both by availability of low-cost high-resolution CCD cameras and ever increasing performance-to-price ratio of personal computers which enables rapid quantitative analysis of the resultant interferograms. The technique offers the advantage of being able to perform non-invasive measurement to the sub-micron level in real-time at video rates enabling continuous deformation of objects under time-varying loads to be analysed.

Ultimately, the optical technique chosen to measure the physical property under test will depend on the required sensitivity and dynamic range.

9 Figures

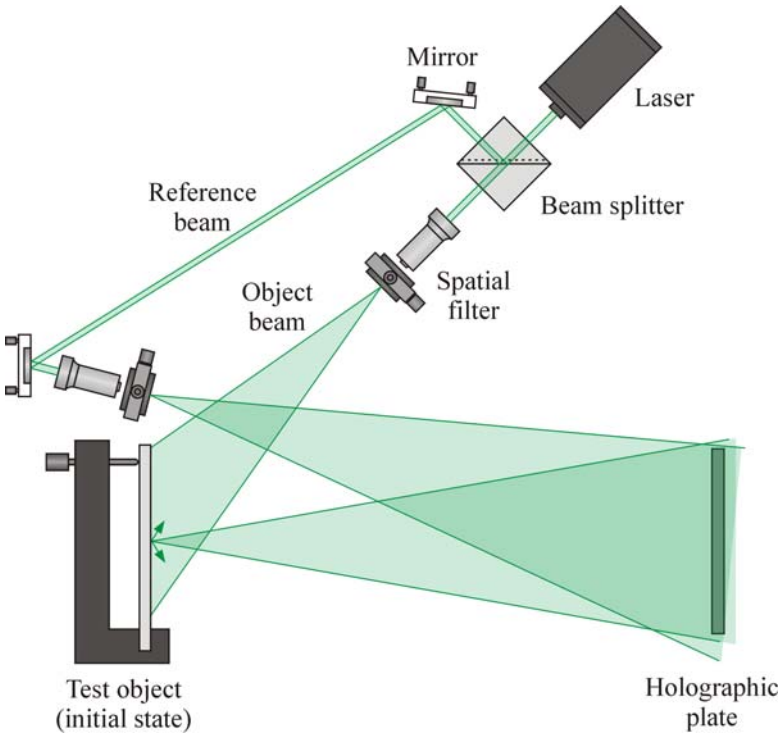

Figure 1: Optical arrangement for recording the initial object state on the holographic plate

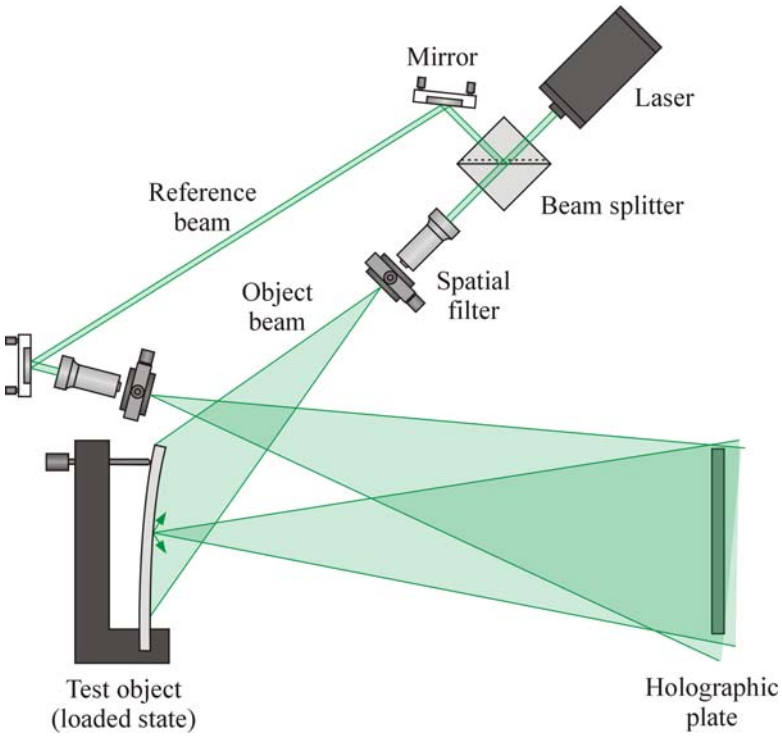

Figure 2: Optical arrangement for recording of the loaded object state on the holographic plate

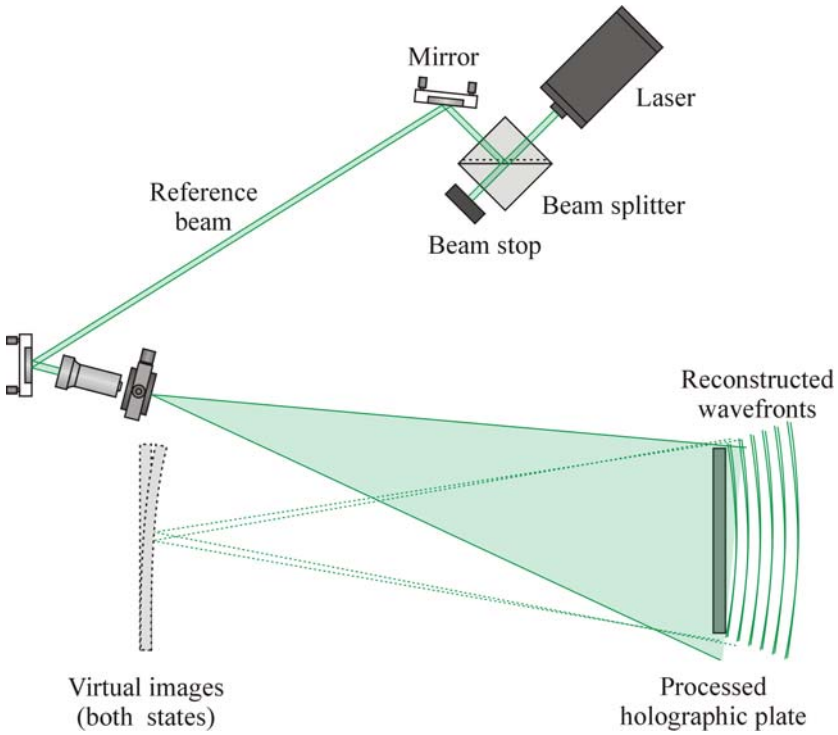

Figure 3: Optical arrangement for reconstruction of a double exposure holographic interferogram

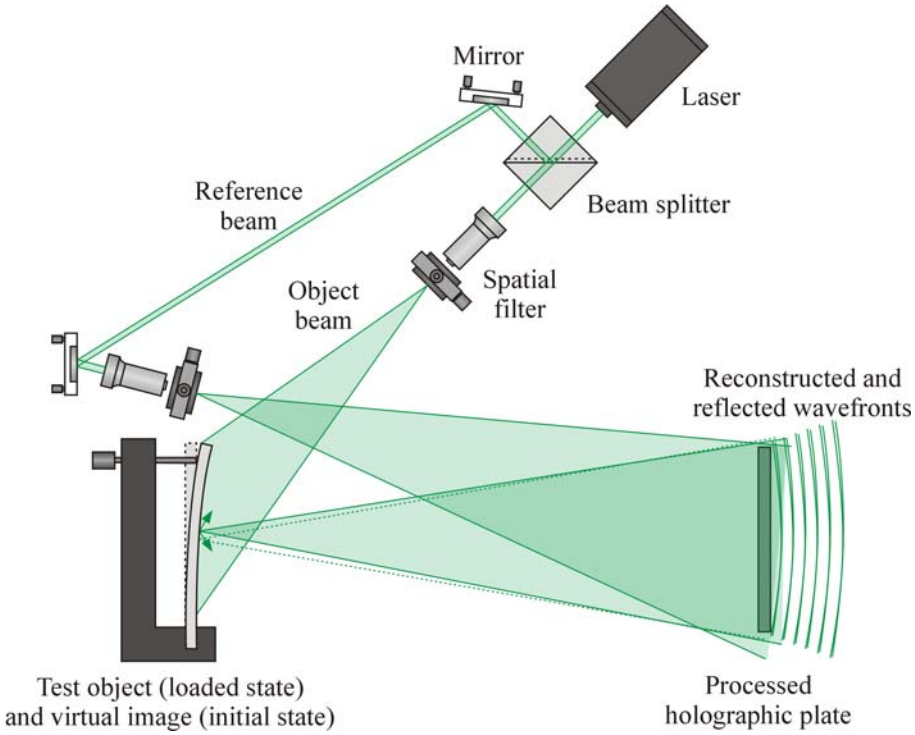

Figure 4: Optical arrangement for reconstruction of a real-time holographic interferogram

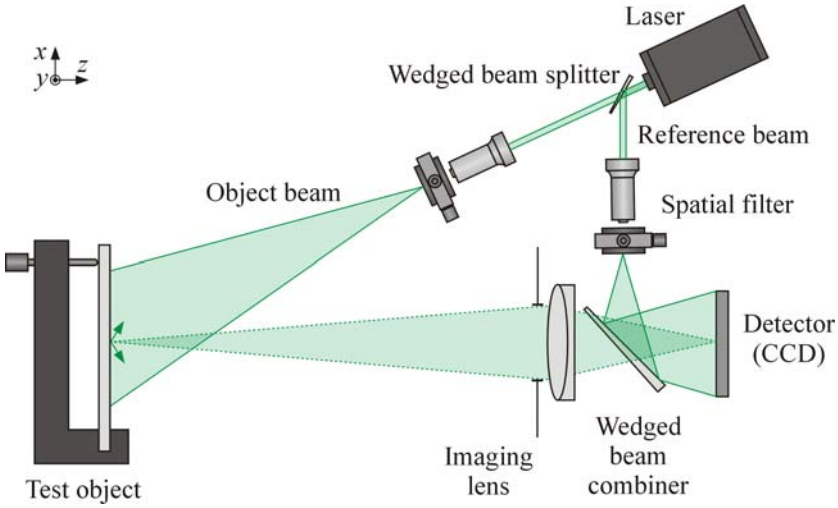

Figure 5: Optical arrangement for out-of-plane speckle interferometry

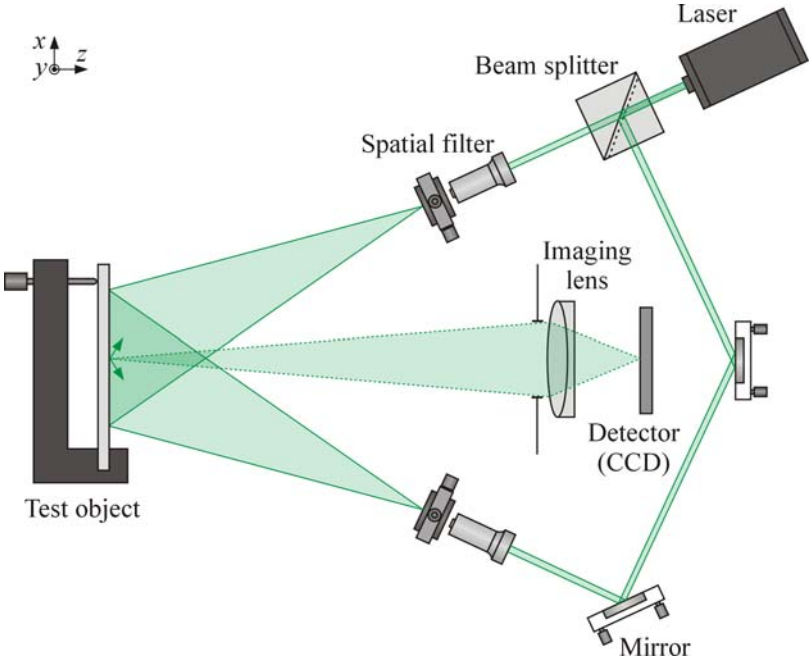

Figure 6: Optical arrangement for in-plane speckle interferometry

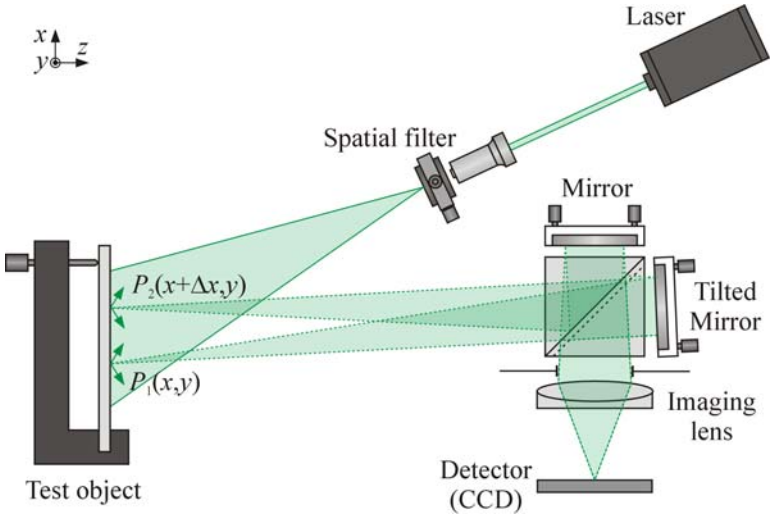

Figure 7: Optical arrangement for speckle shearing interferometry

10 References

1. Sollid J.E. '*Holographic interferometry applied to measurements of small static displacements of diffusely reflecting surfaces*', Applied Optics **8**(8) 1587-1595 (1969).

2. Abramson N. '*The holo-diagram: A practical device for making and evaluating holograms*', Applied Optics **8**(6) 1235-1240 (1969).

3. Jones R., Wykes C. *Holographic and Speckle Interferometry*, Cambridge University Press, Cambridge, 1983.

4. Kreis T. *Holographic Interferometry: Principles and Methods*, Academie Verlag, Berlin, 1996.

5. Vest C.M. *Holographic Interferometry*, John Wiley & Sons, New York, 1979.

6. *Speckle Metrology*, Erf R.K. [Ed], Academic Press, New York, 1978.

7. *Selected Papers on Speckle Metrology*, Sirohi R.S. [Ed], SPIE Optical Engineering Press, Washington, DC, MS 35, 1991.

8. *Speckle Metrology*, Sirohi R.S. [Ed], Marcel Dekker, New York, 1993.

9. Burch J.M., Tokarski J.M.J. '*Production of multi-beam fringes from photographic scatters*', Optica Acta **15** 101-111 (1968).

10. Dandliker R., Jacquot P. 'Holographic interferometry and speckle methods' in *Optical Sensors*, Wagner E., Dandliker R., Spenner K. [Eds], VCH Verlag, Weinheim, 1992, pp. 589-628.

11. Ennos A.E. 'Speckle interferometry', Wolf E. [Ed], North-Holland, Amsterdam, 16, 1978, pp. 233-288.

12. Butters J.N., Leendertz J.A. '*Speckle pattern and holographic techniques in engineering metrology*', Optics & Laser Technology **3** 26-30 (1971).

13. Stetson K.A., Brohinsky W.R. '*Electrooptic holography and its application to hologram interferometry*', Applied Optics **24**(21) 3631-3637 (1985).

14. Wan Abdullah W.S., Petzing J.N., Tyrer J.R. '*Wavefront divergence: a source of error in quantified speckle shearing data*', Journal of Modern Optics **48**(5) 757-772 (2001).

15. Hung Y.Y. 'Displacement and strain measurement' in *Speckle Metrology*, Erf R.K. [Ed], Academic, New York, 1978, p. 55.

16. Joenathan C., Franze B., Tiziani H.J. '*Oblique incidence and observation electronic speckle pattern interferometry*', Applied Optics **33**(31) 7307-7311 (1994).

17. Lokberg O.J., Kwon O. '*Electronic speckle pattern interferometry using a CO2 laser*', Optics & Laser Technology **16**(4) 187-192 (1984).

18. Leendertz J.A. '*Interferometric displacement measurement on scattering surfaces utilizing speckle effect*', Journal of Physics E **3**(3) 214-218 (1970).

19. Leendertz J.A., Butters J.N. '*An image-shearing speckle-pattern interferometer for measuring bending moments*', Journal of Physics E **6** 1107-1110 (1973).

20. Hung Y.Y., Liang C.Y. '*Image-shearing camera for direct measurement of surface strains*', Applied Optics **18**(7) 1046-1051 (1979).

21. Hung Y.Y., Taylor C.G. '*Measurement of slopes of structural deflections by speckle-shearing interferometry*', Experimental Mechanics **14**(7) 281-285 (1974).

22. Gundlach A., Huntley J.M., Manzke B., Schwider J. '*Speckle shearing interferometry using a diffractive optical beamsplitter*', Optical Engineering **36**(5) 1488-1493 (1997).

23. Nakadate S., Yatagai T., Saito H. '*Digital speckle-pattern shearing interferometry*', Applied Optics **19**(24) 4241-4246 (1980).

24. Duffy D.E. '*Moiré gauging of in-plane displacement using double aperture imaging*', Applied Optics **11**(8) 1778-1781 (1972).

25. Hung Y.Y., Rowlands R.E., Daniel I.M. '*Speckle-shearing interferometric technique: a full-field strain gauge*', Applied Optics **14**(3) 618-622 (1975).

26. Murthy R.K., Sirohi R.S., Kothiyal M.P. ' *Speckle shearing interferometry: a new method*', Applied Optics **21**(16) 2865-2867 (1982).

